


RESEARCH ARTICLE

View Article Online
View Journal | View IssueCite this: *Mater. Chem. Front.*,
2019, 3, 1586Received 29th March 2019,
Accepted 24th May 2019

DOI: 10.1039/c9qm00193j

rsc.li/frontiers-materials

A versatile ethanolic approach to metal aerogels (Pt, Pd, Au, Ag, Cu and Co)[†]

Maximilian Georgi, Benjamin Klemmed, Albrecht Benad and
Alexander Eychmüller *

We present a universal one-step approach to generate metal aerogels at room and at dry ice cold temperature, abbreviated as DICE. Performing the synthesis completely in an ethanolic phase allows for the formation of pure noble (Pt, Pd, Au and Ag) and less noble metal (Cu and Co) gels in a remarkably short period of time compared to the widespread aqueous synthesis strategies. Furthermore, three-dimensional disordered, porous networks were obtained for each system with high surface areas of 860 m² mol⁻¹ for Ag up to 5470 m² mol⁻¹ for Co. Additionally, it is shown that the low reaction temperature of -70 °C enables the control of the gelation time without losing the structural characteristics. Moreover, with respect to industrial applications, this facile, stabilizer-free synthesis yields large amounts of materials using highly concentrated precursor solutions.

Introduction

In conjunction with the threat posed by climate change, the focus of the scientific, social and political interest is increasingly shifting towards greater environmental awareness.¹ Promising approaches to convert and store energy without using fossil resources require innovative technologies, especially for electrocatalytic conversion reactions^{2,3} and fuel cell applications.^{4,5} In order to achieve climate goals, a versatile range of high performance materials is required.

An outstanding class of materials are pure noble metal aerogels.⁶ Their homogenous nanoparticulate backbone acts beneficially regarding activities and selectivities in electrocatalytic reactions.^{7,8} Furthermore, the noble metal character and the self-supported structure guarantee a higher (electro-)corrosive resistance and longer durability compared to commercial materials based on carbon.^{9,10} Additionally, the engineering of the materials like varying the particle sizes or shapes or doping with transition metals is not quite exploited yet, but these measures would be promising to increase and to fit the performance to individual reactions.^{11,12} The non-ordered and highly porous networks of metal aerogels combine nanoparticulate properties with easy to handle macroscopic bodies. In addition to the high versatility with regard to their element-specific composition, metal aerogels have the chance to become viable materials for promising applications.

Nevertheless, the production of metal gels is mostly expensive or suffers from difficult procedures. Many approaches require organic solvents, costly and hard to remove additives, and highly diluted solutions.^{13–15}

For quite some years, our group has been working on an aqueous two-step approach for a number of noble mono- and bimetallic aerogels as *e.g.* described by Hermann *et al.*¹⁶ Other approaches use one-step syntheses, either in the presence of stabilizers (for a Au gel¹⁷) or without any capping agents (for *e.g.* Pt, Pd⁹ and other bimetallic PtX gels¹⁸). Furthermore, gelation processes in nonpolar organic solvents *via* the destabilization of a colloidal metal nanoparticle solution with hydrazine, are known.¹⁴ The synthesis of less noble metal aerogels relying on nanosmelting was carried out by Leventis and co-workers.¹⁹

The variety of different approaches and the usage of very large amounts of solvent for the production of small quantities of gels impede the up-scaling of the production. For this reason, work has been done to simplify the metal gel production and enhance their efficiency in applying more universal approaches with, in part, highly concentrated aqueous or non-polar solutions, as shown by the work of Krishna,²⁰ Coaty¹³ and Burpo.²¹

Switching from water or non-polar solvents like hexane to ethanol as a cheap and readily available solvent simplifies the above-mentioned approaches even more. A wide range of metal salt precursors are soluble in ethanol and an additional solvent exchange (like *e.g.* from water to acetone) for supercritical CO₂ drying is not necessary. Furthermore, compared to aqueous solutions the use of ethanol leads to an altered capping and charge stabilization behavior due to its changed permittivity for ions and metal nanoparticles.²²

With regard to the advantages of ethanol as a solvent, we developed a facile and stabilizer-free one-step approach for

Physical Chemistry, TU Dresden, Bergstraße 66b, 01062 Dresden, Germany.
 E-mail: alexander.eychmueller@chemie.tu-dresden.de; Fax: +49 351 463/37164;
 Tel: +49 351 463/39843

[†] Electronic supplementary information (ESI) available: TEM images of a Ni gel and additional characterization results. See DOI: 10.1039/c9qm00193j



noble and less noble metal aerogels reducing highly concentrated metal salt solutions with sodium borohydride (NaBH_4). In order to demonstrate the versatility of our method, gels of noble metals such as Pt, Pd, Au and Ag as well as of less noble metals such as Cu and Co were synthesized. The use of ethanol also allowed a dry ice cold ethanolic (DICE) approach to be performed at -70°C (solid carbon dioxide), as opposed to the more frequently used gelation at slightly elevated temperatures.²³ The obtained aerogels synthesized at different temperatures (room temperature and DICE approaches) were examined with respect to their structure and porosity.

Experimental section

Chemicals

Solids were stored under an inert atmosphere and EtOH (99%, 1% petroleum ether, Berkel AHK) was dried with NaSO_4 before using it to prevent impureness with water. PtCl_4 (99.99%, Alfa Aesar), PdCl_2 (99.999%, Alfa Aesar), $\text{HAuCl}_4 \cdot 3\text{H}_2\text{O}$ (99.9%, Sigma-Aldrich), AgNO_3 (99.9999%, Sigma-Aldrich), CuCl_2 (ultra dry, 99.995%, Thermo Fisher Scientific), NiCl_2 (ultra dry, 99.9%, Alfa Aesar), CoCl_2 (ultra dry, 99.9%, Alfa Aesar), and NaBH_4 (granular, 99.99%, Sigma-Aldrich) were used as received. Each metal salt was dissolved in ethanol to prepare stock solutions of 50 mM.

Synthesis at room temperature

The synthesis of the respective gel system was carried out following the same procedure. In a first step, 2 ml of the metal salt solution (50 mM) was diluted with typically 6 ml EtOH. The solution was kept under N_2 atmosphere by bubbling for a minimum of 20 min. In parallel, sodium borohydride was dissolved in ethanol (50 mM). NaBH_4 was used in a fixed ratio of reduction equivalents to valencies of the metal ion $n_{\text{H}^-} : n_{\text{Me}^+}$ of 4. Subsequently, the prepared reducing agent was injected quickly to the metal salt solution. The color of the respective solution turned immediately to black. After 30 min a black gel sunk completely to the bottom of the beaker. Remaining residues were removed by solvent exchange with an excess of EtOH several times. In a last step, ethanol was exchanged in an autoclave with CO_2 . The carbon dioxide was removed from the pores *via* supercritical drying at 37°C and 90 bar to obtain solid aerogels.

Synthesis at low temperatures (-70°C)

The DICE approach at low temperatures (-70°C) was performed analogously to the room temperature approach, only with use of a cooling bath consisting of a mixture of dry ice and ethanol. The reaction flasks were cooled with this mixture in a Dewar vessel and were removed from the ice bath after adding the reducing agent and waiting for a further 30 minutes. The obtained gels were washed and transferred to aerogels as described above.

Instruments and characterization

For supercritical drying of each metal gel an autoclave, type 13200J0AB from Spi Supplies, was used. To get a first insight into the nanostructured assembly of the gels they were examined by

transmission electron microscopy (TEM) using a JEOL/EO JEM-1400plus equipped with a LaB6 cathode at an acceleration voltage of 120 kV. Followed by checking their homogeneity and porous structure *via* scanning electron microscopy (SEM) with a Hitachi FESEM SU8020 (2 kV, 10 μA). The phases and crystallinity of each gel were studied by powder X-ray diffraction (XRD) using a Bruker Phaser D2 (Cu $K\alpha = 1.5406 \text{ \AA}$) device. Finally, nitrogen adsorption measurements were performed at standard temperatures (77 K) and pressure (1 atm) (STP) to determine the specific surface area (SSA) and total pore volume (TPV) at $p/p_0 = 0.95$ for the aerogels. For this, a Nova3000e from Quantachrome was used.

Results and discussion

Room temperature approach

All syntheses show a similar behavior during the experiment. On adding the reducing agent the colorful solutions immediately turn into dark greyish to black dispersions with a harsh gas evolution. The observations suggest the synproportionation of hydride ions and protons (acidic environment) and the formation of reduced metal species.^{24,25} These small black domains agglomerate quickly and form voluminous cloudy precipitates after a few minutes (for the noble metals) to up to an hour (for the less noble metals). TEM images (Fig. 1) show, that this simple and fast approach leads to products consisting of non-ordered, branched, gel networks for each tested element. It is even possible to extend the range of metal gels using this method, as shown by the synthesis of a Ni gel (Fig. S1, ESI[†]). Each synthesized gel shows interconnected particle chains with a large number of pores, which is typical for metal gels.

Analogous to the description of Bigall *et al.*,²⁶ the primary units of the networks are nanoparticles, which were formed as intermediates during the synthesis, followed by a spontaneous destabilization and gelation.²⁷ Due to the absence of stabilizers and the use of highly concentrated solutions (50–100 times higher than in common approaches) the particles and consequently the network show inhomogeneities and increased nanoparticle (chain) diameters (web thicknesses) compared to those found in the literature.^{9,17} Differences among the gels, like their individual morphologies or variations in the nanoparticle (chain) diameter, result from different reasons. Differences between the metal gels can be caused by their crystal structure, while those of metals with the same crystal structure like Pt, Pd and Ni or Au, Ag and Cu are different due to different reduction rates caused by the metals' individual redox potentials. Additionally the ionic radii of Co, Cu (and Ni) are very small, which influences their mobility.

During the synthesis under inert gas atmosphere in ethanol, a less reactive and protic medium, the gels are protected from oxidation. However, after the supercritical drying the aerogels get in contact with air and start to oxidize. In the case of the Cu and Co aerogels, their metallic backbone is still present after oxidation, although their overall structures changed significantly, *e.g.* the copper strands build needle-like sub-structures⁷ and the cobalt gel surface drastically increases in roughness.





Fig. 1 TEM images of a variety of metal gels synthesized at room temperature via the same ethanolic synthetic approach. Differences in the nanoparticle chain morphologies and diameters are observed depending on the element used. Less noble metals like Cu and Co show substructures due to oxidation.

Using ethanol as a solvent prevents the formation of metal oxide structures during the synthesis due to its reductive effect but also shortens the gelation time significantly. Common synthesis strategies describe durations of several days to weeks between the particle formation, their destabilization and gelation. Liu⁹ reports on an aqueous, stabilizer-free synthesis of a platinum gel with a reduction and gelation time of around 3 weeks. The here produced platinum gels in ethanol need just one hour for the gelation. The shortened reaction time can be explained by the dielectric constant of ethanol compared to that of water.²² Ethanol forms smaller solvation shells around the nanoparticles compared to a hydration shell which results in a less pronounced charge stabilization, leading consequently to a faster destabilization and gelation.

The diffraction patterns (Fig. 2), examined by XRD, show the crystalline phases for each metal aerogel as expected. Only the cobalt gel seems to be completely X-ray amorphous. This amorphous behavior is probably caused by full oxidation of the material. Furthermore, the copper aerogel shows next to its metal phase an additional cuprite phase which is in line with the hypothesis stated above about formation of copper oxide

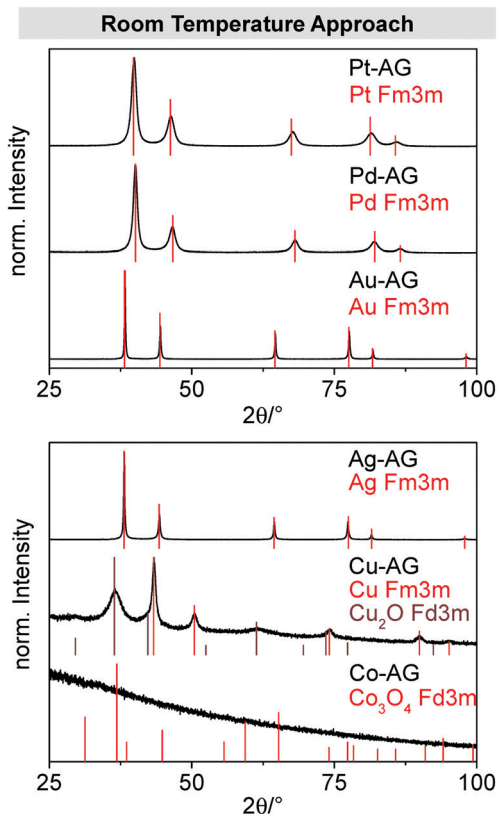


Fig. 2 The noble metal gels synthesized at room temperature show a single metal phase in the XRD, whereas Cu shows an additional oxide phase due to oxidation in air. Co does not show any reflexes because of its amorphous structure.

needles by storing the sample under an oxygen-containing atmosphere. In all cases a reflex broadening is observed which is caused by the small crystallite sizes of the gels.

The beneficial open porous character of the metal gels can be seen in the SEM images (Fig. 3). All aerogels exhibit a three dimensional network with sponge-like morphology. Platinum, palladium and cobalt form a rougher surface, while gold and silver show smooth surfaces, depending on the crystal structure of the metals. In the case of copper, the backbone network is covered with copper oxide needles, as already seen from the TEM image and the XRD pattern.

To get a rough overview about the porosity of the dried metal gels, their densities were estimated and compared to the bulk materials (Table S1, ESI†). For all metal aerogels relative densities of about 0.4% were obtained. Only the gold and silver aerogels show slightly higher relative densities of 1–2%. The increased densities (usually around 0.2% for metal aerogels¹⁶) can be explained by the thicker nanoparticle chains of the gels synthesized by our new approach. To classify the observed porosity of the aerogels, nitrogen adsorption measurements were performed. The specific surface areas were determined in the range of 8 to 38 m² g⁻¹ for the noble metal gels and 75 to 93 m² g⁻¹ (Fig. 1) for copper and cobalt with multipoint Brunauer–Emmett–Teller (BET) plots (Fig. 4). The large range in the surface areas between the noble and less noble metal gels can be explained



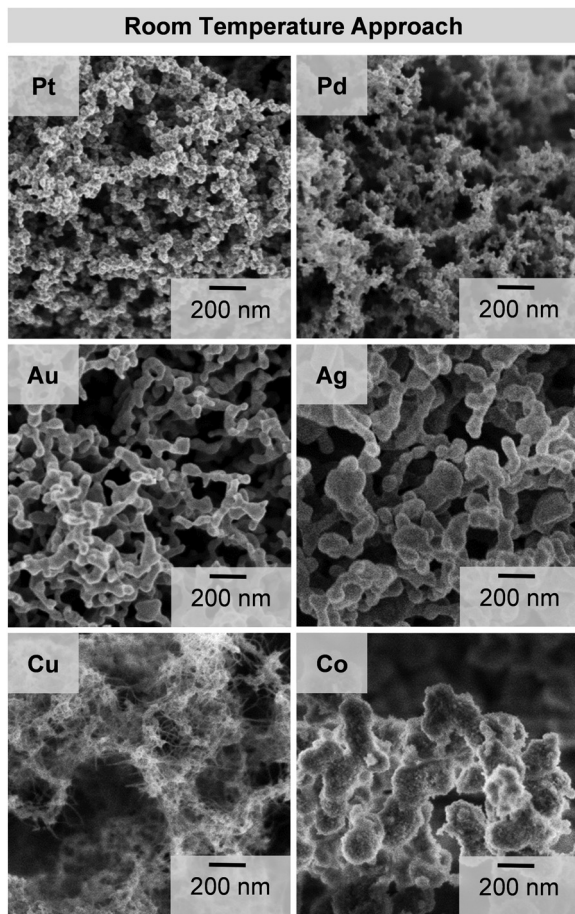


Fig. 3 SEM images of aerogels, similarly synthesized by the room temperature approach. The gels consist of open porous three dimensional networks with specific element dependent morphologies.

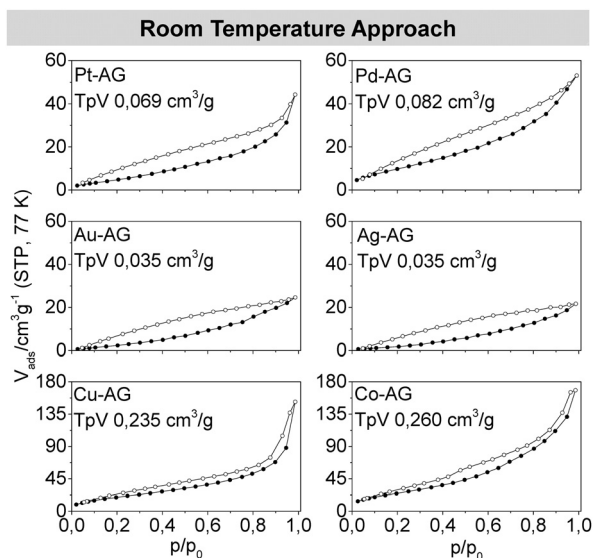


Fig. 4 Isotherms measured by nitrogen physisorption at STP (standard temperature at 77 K and pressure) for the metal aerogels synthesized at room temperature. The isotherms show characteristics of Type II/IV due to the presence of a wide range of pores (TPV = total pore volume).

by the oxidation of copper and cobalt. The formation of the oxidic substructure leads to a more branched and rougher gel network with an increased surface area. The differences between the noble metals among each other have several reasons. The surface area is most strongly influenced by the diameter of the web thickness of a gel with the same basic structure. A high web thickness leads to lower surface areas, as the gold and silver gels show, in comparison to the smaller palladium and platinum gels. Additionally, these two gels form rougher and rugged surfaces which further increases the surface areas. When considering the mass-related specific surfaces, it should also be considered that the gels of different elements have very different molar masses. Therefore, also the surface area per mole was calculated to simplify the comparison of the gels (see also Fig. 9).

Each of the metal aerogel isotherms measured by nitrogen physisorption shows characteristics of a type II isotherm, mixed with characteristics of a type IV isotherm. This mixture is caused by the presence of both mesopores (2–50 nm) and macropores (>50 nm) generated by interparticulate spaces between the strands. Thus, the aerogels show typical behavior. However, the big differences between the adsorption and desorption branches in the area of p/p_0 lower than 0.42 are non-typical. Both graphs should cross each other in this area, since multi-layer adsorptions are unlikely due to the low relative pressure. Already known is the percolation through bottleneck pores, bigger pores which are surrounded by smaller ones, but this effect is unexpected due to the wide pore-size distributions as presented here.²⁸ Another, more likely explanation implies an elastic behavior of the whole porous system, while the network expands during the adsorption and shrinks to its initial size by desorption. This breathing-like behavior also explains the overlap of the adsorption and desorption branches for some of the measurements.^{28,29} This assumption corresponds with the measurements and calculations from Reichenauer *et al.* which as well predict an elastic behavior of silica aerogels from isotherm data.^{30,31} The pore size distribution of all metal aerogels was assessed with the Barrett–Joyner–Halenda (BJH) method (Fig. S2, ESI†). All metal aerogels show the expected wide range of pore sizes, which due to the minimizing of the diffusion barriers is ideal for material transport reactions. In addition to the presence of meso- and macropores, pores smaller than 2 nm were detected. Due to deviations in the BJH method, these small pores are attributable to surface roughness and the primary building blocks.

Compared with other universal synthetic approaches for porous metal-gel-like structures our presented synthesis is superior due to its flexibility, simplicity and high degree of porosity,^{13,20,21} increasing the attractiveness of metal aerogels. In comparison, highly optimized aerogels show even larger porosity and homogeneity with the disadvantage of being inappropriate for large-scale productions and applications due to their need of highly diluted solutions and additional stabilizers during the synthesis procedure.

Low temperature approach

Analogous to the room temperature approach, the formation of black dispersions and evolution of gas after adding NaBH_4 to the respective metal salt solutions are also observable in the



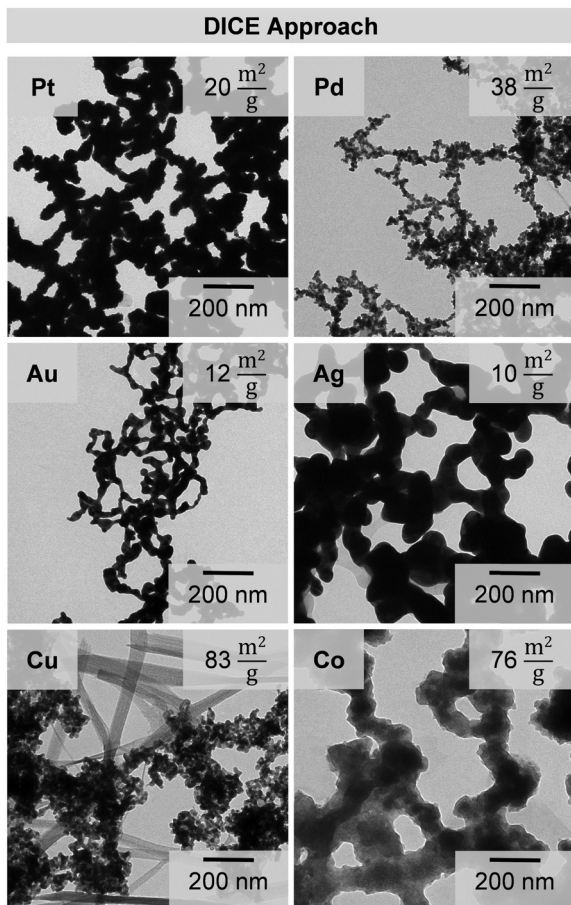


Fig. 5 TEM images of gels for a wide range of metals synthesized at low temperatures via the same synthetic approach as above. Differences in the nanoparticle chain diameters are specific for every metal and result in different specific surface areas. Less noble metals show oxidized substructures.

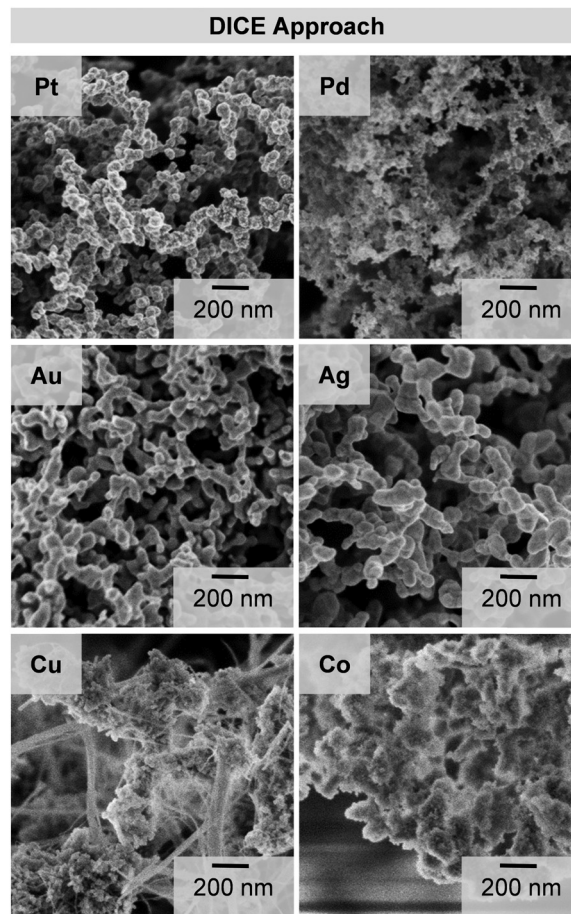


Fig. 6 SEM images of aerogels, synthesized by the similar dry ice cold ethanolic (DICE) approach. The gels consist of highly, open porous, three dimensional networks with specific element dependent morphologies. The low temperatures do not affect the structure of the aerogels.

DICE approach. However, the coloration occurred gradually and not in one step which indicates retarded kinetics of the reaction. Moreover, the gelation is stopped or at least delayed when the reaction solution is stored in the cooling bath because no agglomeration is observable (Fig. S3, ESI[†]). Only the removal of the samples from the cooling bath (in this case stopped after 150 min) allows the formation of the voluminous precipitates analogous to the room temperature approach. This observation confirms again the assumption of slowed down kinetics at low temperatures for the gelation. Similar to the room temperature approach, the intermediately formed primary units of the respective metal connect to gel networks, whereby Cu and Co show again oxidized substructures (Fig. 5). The slowed down kinetics do not affect the gelation process itself and the simple and flexible character of the synthetic approach remains. We observed similar web thicknesses in both the room temperature and DICE approaches (Fig. S4, ESI[†]). Pd, Au, Ag and Cu do not show significant differences regarding the average diameter of the nanoparticle chains (5%), while the diameter increases for Pt, and decreases for Co up to 50% on average.

The SEM images (Fig. 6) show the presence of open porous three dimensional, sponge-like structures for each metal aerogel

synthesized by the DICE approach. The structure of the gels remains unaltered even though the kinetics of the gelation are slowed down.

The synthesis at $-70\text{ }^{\circ}\text{C}$ also preserves the crystalline properties of the aerogels (Fig. 7). Pt, Pd, Au and Ag show the reflexes of the pure metals. The Cu aerogel oxidizes while stored under air and shows an additional cuprite phase, while cobalt seems to be completely amorphous.

The similarity between the room temperature and DICE approaches is also reflected by the almost identical estimated relative densities (Table S1, ESI[†]) and the nitrogen physisorption results. They indicate a broad range of pores with the typical characteristics of Type II and IV isotherms in the measured nitrogen isotherms (Fig. 8). Even the elastic behavior is reflected again in the isotherms. The estimated pore size distributions (Fig. S2, ESI[†]) do not differ significantly from those of the room temperature approach.

Fig. 9 shows the comparison of the SSA and TPV between the room temperature and DICE approaches for the respective gels of all elements.

Both characteristic parameters show large similarities. Only the two less noble metals Cu and Co behave differently due to





Fig. 7 XRD patterns for each synthesized metal gel *via* the DICE approach. The gels behave similar to the room temperature approach. Noble metal gels show a single metal phase, whereas Cu exhibits an additional oxide phase due to oxidation under air. Co does not display any reflexes because of its amorphous structure.

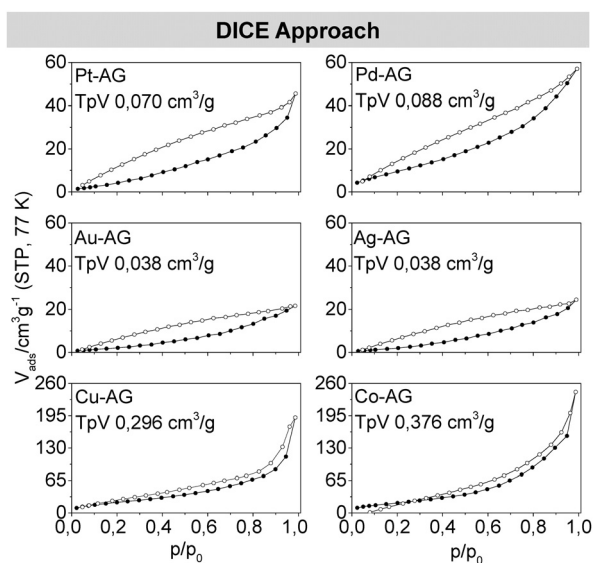


Fig. 8 Isotherms measured by nitrogen physisorption at STP (standard temperature at 77 K and pressure) for the metal aerogels synthesized at dry ice cold temperature. The isotherms show characteristics of Type II/IV due to the presence of a wide range of pore sizes. The large differences between the adsorption and desorption branches indicate an elastic behaviour of the gels.

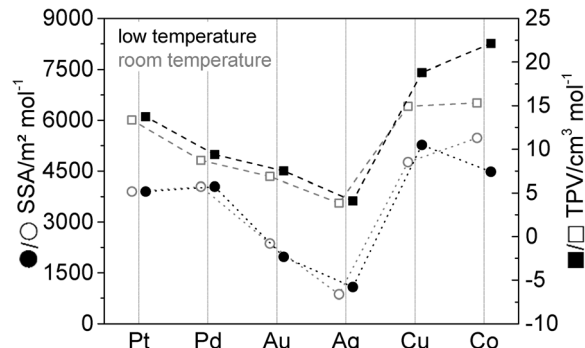


Fig. 9 Comparison of the specific surface areas and total pore volumes of all synthesized metal aerogels, revealed by nitrogen physisorption measurements. The almost identical porous appearance reflects the structural equality of the respective gels synthesized by the room temperature and DICE approaches.

the oxidation of both metals under air. We assume that Cu, as a more noble metal than cobalt, only oxidizes on the surface of the nanoparticle chains, whereby the oxide shell passivates the gel. In the case of cobalt, the complete gel oxidizes due to its lower standard potential. In addition to the high temperature gradient to which the material is exposed during the DICE approach, parts of the Co gel collapse and the surface area decreases.

All aerogels produced (by the RT and DICE approaches) were photographed after their syntheses. The majority of the partly powdery samples show a dark color (Fig. S5, ESI†). They differ from the bulk material, due to their nanoparticulate substructure. In general there are no differences in color for the aerogels synthesized at the two temperatures. Pt and Pd show typically black color, whereas the Au aerogel is brownish-red to black. This mixture is caused by the inhomogeneous diameter of the nano-chains. The brownish color indicates thicker structures, such as those found in the SEM images. The silver aerogel is also grey due to its larger web thickness. The copper gel, on the other hand, is black for the room temperature approach, but has a green tint for the DICE approach. This is a result of the differently progressing oxidation of the materials. The same phenomenon is responsible for the different coloring of the cobalt aerogels.

Conclusions

In summary, we report a universal and fast approach for noble and less noble metal aerogels in ethanol at room temperature and DICE. With this universal and facile method we are able to produce a wide range of pure metal gels, like Pt, Pd, Au, Ag, Cu and Co. The ethanol acts beneficially due to the low boiling point and the low dielectric constant compared to water which is used in the more conventional syntheses. Thereby, the metal salt concentration is high, the gelation time is significantly shortened and a control of the gelation time is given *via* the temperature control. The supercritically dried noble metal gels show surface areas from 860 m² mol⁻¹ for Ag to 4043 m² mol⁻¹ for Pd, depending on the diameter of the nanoparticle chains and the substructure of the respective gel. In contrast, less noble metal aerogels based on Cu or Co have the tendency to oxidize



which leads to a change of the nanostructure and thus to an unexpected increase of the surface area to $5477 \text{ m}^2 \text{ mol}^{-1}$.

In future the same procedure will be used for other metals and for bimetallic systems. Besides that, slight optimizations for each metal relating to e.g. the ratio of sodium borohydride to metal ions can lead to thinner structures with a higher porosity. Low temperature techniques associated with the slowing down of the reaction are promising to gain deeper insight into the gelation mechanism. Furthermore, the slowed down reaction at dry ice cold temperatures opens up new synthetic possibilities, such as the simple modification of the intermediate nanoparticles before the gelation. This aspect becomes particularly interesting when noble and less noble metals are combined to create substructures in the obtained gel, which in turn can significantly improve the catalytic activity compared to current catalysts. Until now, these modifications were only possible by more complex multi-step approaches and the addition of further reactants. Our presented synthesis enhances the attractiveness of metal aerogels for a wide range of applications, especially on large scales. This new method allows the production of larger quantities of aerogel in a short time compared to the current synthesis methods. One batch yields as much gel as in current syntheses. But the shortened gelation time and the lower reaction volume make it very easy to carry out several batches in parallel, which significantly improves the production efficiency. Furthermore, upscaling of the method is not limited as long as a rapid mixing of the reactants is carried out.

Conflicts of interest

There are no conflicts of interest to declare.

Acknowledgements

We thank the Swiss National Science Foundation (SNF) and the Deutsche Forschungsgemeinschaft (German Research Foundation) (DFG EY 16/18-2) for financial support as well as the European Research Council (ERC AdG 2013 AEROCAT).

Notes and references

- S. Solomon, G. Plattner, R. Knutti and P. Friedlingstein, *Proc. Natl. Acad. Sci. U. S. A.*, 2009, **106**, 1704–1709.
- W. Wang, S. Wang, X. Ma and J. Gong, *Chem. Soc. Rev.*, 2011, **40**, 3703–3727.
- E. E. Benson, C. P. Kubiak, A. J. Sathrum and J. M. Smieja, *Chem. Soc. Rev.*, 2009, **38**, 89–99.
- D. G. Nocera and M. P. Nash, *Proc. Natl. Acad. Sci. U. S. A.*, 2007, **104**, 15729–15735.
- S. M. Haile, *Acta Mater.*, 2003, **51**, 5981–6000.
- C. Ziegler, A. Wolf, W. Liu, A. K. Herrmann, N. Gaponik and A. Eychmüller, *Angew. Chem., Int. Ed.*, 2017, **56**, 13200–13221.
- S. Henning, L. Kühn, J. Herranz, M. Nachtegaal, R. Hübner, M. Werheid, A. Eychmüller and T. J. Schmidt, *Electrochim. Acta*, 2017, **233**, 210–217.
- S. Henning, J. Herranz, H. Ishikawa, B. J. Kim, D. Abbott, L. Kühn, A. Eychmüller and T. J. Schmidt, *J. Electrochem. Soc.*, 2017, **164**, F1136–F1141.
- W. Liu, P. Rodriguez, L. Borchardt, A. Foelske, J. Yuan, A. K. Herrmann, D. Geiger, Z. Zheng, S. Kaskel, N. Gaponik, R. Kötz, T. J. Schmidt and A. Eychmüller, *Angew. Chem., Int. Ed.*, 2013, **52**, 9849–9852.
- M. Zareie Yazdan-Abad, M. Noroozifar, A. R. Modaresi Alam and H. Saravani, *J. Mater. Chem. A*, 2017, **5**, 10244–10249.
- B. Cai, A. Dianat, R. Hübner, W. Liu, D. Wen, A. Benad, L. Sonntag, T. Gemming, G. Cuniberti and A. Eychmüller, *Adv. Mater.*, 2017, **29**, 1605254.
- B. Cai, D. Wen, W. Liu, A. K. Herrmann, A. Benad and A. Eychmüller, *Angew. Chem., Int. Ed.*, 2015, **54**, 13101–13105.
- C. Coaty, H. Zhou, H. Liu and P. Liu, *ACS Nano*, 2018, **12**, 432–440.
- S. Naskar, A. Freytag, J. Deutsch, N. Wendt, P. Behrens, A. Köckritz and N. C. Bigall, *Chem. Mater.*, 2017, **29**, 9208–9217.
- D. Wen, A. K. Herrmann, L. Borchardt, F. Simon, W. Liu, S. Kaskel and A. Eychmüller, *J. Am. Chem. Soc.*, 2014, **136**, 2727–2730.
- A. K. Herrmann, P. Formanek, L. Borchardt, M. Klose, L. Giebeler, J. Eckert, S. Kaskel, N. Gaponik and A. Eychmüller, *Chem. Mater.*, 2014, **26**, 1074–1083.
- D. Wen, W. Liu, D. Haubold, C. Zhu, M. Oschatz, M. Holzschuh, A. Wolf, F. Simon, S. Kaskel and A. Eychmüller, *ACS Nano*, 2016, **10**, 2559–2567.
- S. Henning, H. Ishikawa, L. Kühn, J. Herranz, E. Müller, A. Eychmüller and T. J. Schmidt, *Angew. Chem., Int. Ed.*, 2017, **56**, 10707–10710.
- N. Leventis, N. Chandrasekaran, C. Sotiriou-Leventis and A. Mumtaz, *J. Mater. Chem.*, 2009, **19**, 63–65.
- K. S. Krishna, C. S. S. Sandeep, R. Philip and M. Eswaremoorthy, *ACS Nano*, 2010, **4**, 2681–2688.
- F. J. Burpo, E. A. Nagelli, L. A. Morris, J. P. McClure, M. Y. Ryu and J. L. Palmer, *J. Mater. Res.*, 2017, **32**, 4153–4165.
- M. Mohsen-Nia, H. Amiri and B. Jazi, *J. Solution Chem.*, 2010, **39**, 701–708.
- Q. Shi, C. Zhu, D. Du, C. Bi, H. Xia, S. Feng, M. H. Engelhard and Y. Lin, *J. Mater. Chem. A*, 2017, **5**, 19626–19631.
- D. L. Van Hyning and C. F. Zukoski, *Langmuir*, 1998, **14**, 7034–7046.
- Y. Song, R. M. Garcia, R. M. Dorin, H. Wang, Y. Qiu, E. N. Coker, W. A. Steen, J. E. Miller and J. A. Shelnut, *Nano Lett.*, 2007, **7**, 3650–3655.
- N. C. Bigall, A. K. Herrmann, M. Vogel, M. Rose, P. Simon, W. Carrillo-Cabrera, D. Dorfs, S. Kaskel, N. Gaponik and A. Eychmüller, *Angew. Chem., Int. Ed.*, 2009, **48**, 9731–9734.
- N. C. Bigall and A. Eychmüller, *Philos. Trans. R. Soc., A*, 2010, **368**, 1385–1404.
- M. Thommes, *Chem. Ing. Tech.*, 2010, **82**, 1059–1073.
- J. L. Mohanan, I. U. Arachchige and S. L. Brock, *Science*, 2005, **307**, 397–400.
- G. Reichenauer and G. W. Scherer, *J. Colloid Interface Sci.*, 2001, **236**, 385–386.
- G. Reichenauer and G. W. Scherer, *J. Non-Cryst. Solids*, 2001, **285**, 167–174.

